Applied Catalysis B: Environmental 247 (2019) 182–190

Contents lists available at ScienceDirect

Applied Catalysis B: Environmental

journal homepage: www.elsevier.com/locate/apcatb

Design and catalytic applications of 1D tubular nanostructures: Improving efficiency in glycerol conversion

Lucia A. Bivona[a,1], Alvise Vivian[a,1], Luca Fusaro[a], Sonia Fiorilli[b], Carmela Aprile[a,*]

[a] Unit of Nanomaterials Chemistry, Department of Chemistry, University of Namur, 5000 Namur, Belgium
[b] Department of Applied Science and Technology, Polytechnic of Turin, Corso Duca degli Abruzzi, 24, 10129 Torino, Italy

ARTICLE INFO

Keywords:
Glycerol valorization
Solketal
Lactates
Nanotubes
Tin

ABSTRACT

The design of novel and efficient heterogeneous catalysts represents one of the main challenges in the development of sustainable processes. A straightforward one-pot sol-gel approach for the controlled preparation of highly active 1D nanotubes is herein presented. The optimization of the synthesis parameters allowed obtaining materials with tubular structure and very high surface area even in the absence of additional hydrothermal treatments hence further reducing the environmental impact of the synthesis approach. The isomorphic substitution of Sn within the silica framework was assessed via ^{119}Sn solid state NMR under static conditions. Sn-silica nanotubes were efficiently used to catalyze both the transformation of dihydroxyacetone into ethyl lactate and the conversion of glycerol into solketal, where outstanding turnover frequencies were obtained under solvent-free conditions. The catalytic performance of these materials is ascribed to the enhanced accessibility of their active sites given by their tubular morphology and to the suitable combination of acid sites. Moreover, no-leaching of active sites was evidenced and the best solid preserved its activity in multiple catalytic cycles. Characterization after the reuses allows supporting further the stability of tin-nanotubes under the selected reactions conditions.

1. Introduction

Nowadays, heterogeneous catalysis plays more than ever a pivotal role in the development of a more sustainable society in which chemicals, materials and energy are produced considering both resource efficiency and waste minimization [1]. In this context, the development of novel and highly efficient catalysts represents one of the main challenges attracting the attention of the scientific community. Since they can be easily separated from products and unreacted starting materials, reactivated and reused in consecutives cycles, heterogeneous catalysts constitute a valid alternative to standard non-catalyzed process as well as to homogeneous catalysis. Their major drawback is represented by the diffusion limitations that reactants and products may encounter while approaching or leaving the active sites. Hence, considerable efforts are dedicated to the design of novel heterogeneous catalysts able to enhance the accessibility of highly dispersed and well-defined active centers in order to simulate the behavior of the homogeneous ones. As a result, a large variety of approaches ranging from the reduction of the catalysts particle size and modification of their shape [2–4] to the synthesis of highly porous materials [5,6] have been investigated. Due to their high chemical and thermal stability as well as the relatively easy synthesis procedure allowing a careful control of the textural and structural features, silica based solids are probably the most used supports for catalytic purposes. A plethora of high surface area silicates with tunable pore size ranging from microporous crystalline solids (zeolites) to mesoporous materials (e.g. MCM-41, SBA-15, TUD-1) [6–8] have been synthesized and efficiently employed to catalyze various chemical reactions. In the broad series of porous silicates, the controlled preparation of nanotubes constitutes a recent advancement. In 1999, Harada and Adachi [9] reported a sol-gel method for the synthesis of single silica nanotubes or bundles through a surfactant-mediated template mechanism and they described the procedure for controlling the geometry of the tubes. Earlier research showed that mixtures of commercially available triblock copolymer surfactants of the Pluronics family, in the presence of a micelle swelling agent, are effective templates for the synthesis of silica nanotubes with adjustable inner diameter [10,11]. These open-ends tubular nanostructures display promising features as supports in heterogeneous catalysis. Moreover, the possibility to reduce the tubes to a tailored short length would ideally facilitate mass transport resulting in a consequently higher productivity [12].

Concerning the possible applications, in the field of green

* Corresponding author.
E-mail address: carmela.aprile@unamur.be (C. Aprile).
[1] These authors contributed equally to this work.

https://doi.org/10.1016/j.apcatb.2019.01.085
Received 3 September 2018; Received in revised form 19 January 2019; Accepted 29 January 2019
Available online 30 January 2019
0926-3373/

chemistry, it was already pointed out that some starting materials may come from bio-sources and can be produced via a low energy consumption and reduced costs strategies compared to standard petrochemical-based reactants. Glycerol represents one of the most abundant biomass derived product. The conversion of glycerol and its derivatives to added-value chemicals is receiving a considerable attention due to the growing interest for biodiesel as alternative to fossil fuels. Biodiesel production is based on the transesterification of triglycerides obtained from natural lipids and yields glycerol as the main co-product. In this context, porous silicates embedding different metal elements (Sn, Ga, Zr…), partially substituting silicon in their framework, have been reported as active and selective catalysts for the conversion of glycerol and its oxidation derivative (dihydroxyacetone) to solketal and ethyl lactate respectively [4,13–15]. Glycerol through an acetalization reaction with acetone can be converted to solketal, which has direct applications as surfactant, fuel additive and flavoring agent [16–18]. The acetalization reaction is typically catalysed by Brønsted acids, [19–21] though metal-substituted mesoporous silicates displaying mainly Lewis acidity have also been reported as promising heterogeneous catalysts for this reaction [22]. Another relevant process is represented by the conversion of trioses such as dihydroxyacetone (DHA), obtained from glycerol via catalytic processes, to ethyl lactate. This attractive product can be employed as green solvent, as precursor for the synthesis of polylactic acid and in various other applications related to food, pharmaceutical and cosmetic industry [23–25]. This second reaction is also catalyzed by a combination of Brønsted and Lewis acidity, with the former promoting the dehydration of dihydroxyacetone to pyruvic aldehyde, and the latter catalyzing the rearrangement of this intermediate to ethyl lactate [26].

Herein, we harness the opportunity offered by the unique morphology of inorganic nanotubes to synthesize in a one pot sol-gel approach highly active Sn-silica nanotubes which were efficiently used to catalyze both the conversion of glycerol into solketal and the transformation of dihydroxyacetone into ethyl lactate. To the best of our knowledge we report here for the first time the controlled insertion of Sn as single site in the framework of silica nanotubes synthesized using a surfactant templated sol-gel approach.

2. Experimental part

2.1. Materials and methods

Transmission electron microscopy (TEM) images were taken using a Philips Tecnai 10 microscope operating at 80 kV. Nitrogen adsorption-desorption analysis were carried out at 77 K with a volumetric adsorption analyzer (Micromeritics Tristar 3000). Prior to the analysis, the samples were pre-treated at 150 °C overnight under reduce pressure (0.1 bar). The Brunauer–Emmet–Teller (BET) method was applied in the 0.05–0.20 P /P_0 range to calculate the specific surface area. Inductively coupled plasma optical emission spectroscopy was employed to quantify the metal (tin) in the materials using an Optima 8000 ICP-OES Spectrometer. The Si environment and the coordination of the Sn atoms were studied by ^{29}Si Magic Angle Spinning (MAS-NMR) and static ^{119}Sn Nuclear Magnetic Resonance. ^{29}Si NMR spectra were recorded at room temperature on a Bruker Avance-500 spectrometer operating at 11.7 T (99.3 MHz for ^{29}Si) using a 4 mm CP-MAS Bruker probe. The sample was packed in a 4 mm zirconia rotor and measured with a spinning frequency of 8000 Hz. Quantitative ^{29}Si spectra were recorded using the following acquisition parameters: 300 s relaxation delay, 3μs (90°) excitation pulse, 52 ms acquisition time. CP-MAS spectra were recorded using a 5 s relaxation delay and 5 ms contact time. The processing comprised exponential multiplication of the FID with a line broadening factor of 30 Hz, zero-filling, Fourier transform, phase and baseline corrections. The chemical shift scale was calibrated at room temperature with respect to a sample of solid 3-(Trimethylsilyl)-1-propanesulfonic acid sodium salt (DSS) (0.0 ppm).

^{119}Sn NMR spectra were recorded at room temperature on a Varian VNMRS-400 spectrometer operating at 9.4 T (149 MHz for ^{119}Sn) using a 10 mm wideline probe. The sample was packed in a 10 mm Kel-F tube and studied in static condition. ^{119}Sn spectra were recorded using the Hahn echo pulse sequence and following acquisition parameters: 60 s relaxation delay, 3μs (90°) excitation pulse, 5 ms acquisition time. The processing comprised exponential multiplication of the FID with a line broadening factor of 1000 Hz, zero-filling, Fourier transform, phase and baseline corrections. The chemical shift scale was calibrated at room temperature with respect to the isotropic shift of SnO_2 to -603 ppm [43].

Brønsted and Lewis acidity of the samples Sn-NTs-A and Sn-NTs-B was investigated by Fourier Transform Infrared Spectroscopy (FT-IR) of ammonia adsorption. FT-IR measurements were performed in transmission mode by using a Bruker Tensor 27 spectrometer equipped with a liquid nitrogen-cooled mercury–cadmium–telluride (MCT) detector, operating at 2 cm^{-1} resolution. Pre-treatments were carried out using a standard vacuum frame, in an IR cell equipped with KBr windows. The samples were pressed into self-standing wafers and outgassed 1 h at 400 °C before adsorption of ammonia at room temperature.

Adsorption of ammonia was studied in the pressure range 0.01–20.0 mbar: the reversible fraction of the adsorbed ammonia was then removed by prolonged outgassing at room temperature.

All the components for the conversion of DHA into EL were analyzed by Gas chromatography on a Trace GC Ultra from Interscience, with a polar column (phase: PH M-1, 0.5 μm, 5.0 m, 0.32 mm) using nitrogen as carrier gas at constant flow rate of 2.0 mL/min. The oven temperature was maintained at 50 °C for 2 min, then increased to 300 °C at 200 °C/min and finally maintained at 300 °C for 1.23 min. Concerning the condensation reaction of acetone with glycerol, all the components were analysed by NMR recorded in liquid state and using DMSO as deuterated solvent.

2.2. Synthesis of Sn-NTs

Sn-NTs-A: Pluronic F127 ($EO_{106}PO_{70}EO_{106}$, $0.8{\cdot}10^{-4}$ mol, 1.0 g) was transferred in a covered container in PP and dissolved in 2 N HCl (60.0 mL) at 11 °C, under stirring at 250 rpm for 1 h. Then, a solution of $SnCl_4{\cdot}5\ H_2O$ ($3.51{\cdot}10^{-4}$mol, 0.123 g, Si/Sn = 37) in absolute ethanol (0.2 mL) was mixed with TEOS (0.013 mol, 2.8 g) and toluene (3.0 mL) and added dropwise at 11 °C. The reaction mixture was stirred at 250 rpm for 24 h at 11 °C. After this, it was treated hydrothermally for 24 h at 100 °C. The as-synthetized material (gel) was filtered, washed with milli Q water (600 mL) and dried at 65 °C in an oven overnight. The resulting white powder was calcined at 550 °C under air for 5 h (heating ramp 2 °C/min).

Sn-NTs-B: Pluronic F127 ($EO_{106}PO_{70}EO_{106}$, $0.8{\cdot}10^{-4}$ mol, 1.0 g) was transferred in a covered container in PP and dissolved in 2 N HCl (60.0 mL) at 11 °C, under stirring at 250 rpm for 1 h. Then, a solution of $SnCl_4{\cdot}5\ H_2O$ ($3.51{\cdot}10^{-4}$mol, 0.123 g, Si/Sn = 37) in absolute ethanol (0.2 mL) was mixed with TEOS (0.013 mol, 2.8 g) and toluene (3.0 mL) and added dropwise at 11 °C. The reaction mixture was stirred at 250 rpm for 24 h (Sn-NTs-B). The as-synthetized material (gel) was filtered, washed with milli Q water (600 mL) and dried at 65 °C in an oven overnight. The resulting white powder was calcined at 550 °C under air for 5 h (heating ramp 2 °C/min).

2.3. Catalytic tests

Conversion of dihydroxyacetone to ethyl lactate: DHA (180.0 mg, $2{\cdot}10^{-3}$ mol), decane (25.0 mg, $0.2{\cdot}10^{-3}$ mol, GC internal standard) and absolute EtOH (3.92 g, 5.0 mL) were weighed inside a 25 mL glass vial. Then, DHA was dissolved in EtOH during 30 min at 50 °C under 800 rpm. Then, the catalyst was added to the mixture. The reaction mixture was heated at 90 °C under 1200 rpm. At the end of the catalytic test, the mixture was cooled down at room temperature and centrifuged

(10 min, 4500 rpm). After, a sample of the supernatant was analyzed by gas chromatography on a Trace GC Ultra.

Conversion of dihydroxyacetone to ethyl lactate (preparative test): DHA (90.0 mg, $1{\cdot}10^{-3}$ mol), decane (12.5 mg, 0.1 $\cdot 10^{-3}$ mol, GC internal standard) and absolute EtOH (1.96 g, 2.5 mL) were weighed inside a 25 mL glass vial. Then, DHA was dissolved in EtOH during 30 min at 50 °C under 800 rpm. Then, Sn-NTs-B (50.0 mg) was added to the mixture. The reaction mixture was heated at 90 °C under 1200 rpm for 24 h. At the end of the catalytic test, the mixture was cooled down at room temperature and centrifuged (10 min, 4500 rpm). After, a sample of the supernatant was analyzed by gas chromatography on a Trace GC Ultra.

Leaching tests: For the leaching tests, DHA (90.0 mg, $1{\cdot}10^{-3}$ mol) was dissolved in absolute EtOH (1.97 g, 2.50 mL) containing decane (13.9 mg, $1{\cdot}10^{-4}$ mol) at 50 °C for 30 min under 800 rpm stirring. Then, Sn-NTs-B catalyst (50 mg) was added and the reaction mixture was heated at 90 °C under 1200 rpm stirring. After 1 h, the catalyst was separated from the reaction mixture by hot filtration (~ 90 °C). A sample of the filtrate (0.20 mL) was taken for GC analysis (diluted 5 times in EtOH prior to GC analysis). The filtrate was kept at 90 °C for another 5 h 30 min. A second GC analysis of the reaction mixture was then performed.

Acetalyzation of acetone with glycerol: In a round bottom flask, glycerol (purity 99%, 921 mg, $1{\cdot}10^{-2}$ mol), acetone (2.32 g, 4 equiv.) 1,4-dioxane (132 mg, $1.5{\cdot}10^{-3}$ mol, as GC internal standard) and Sn-NTs-B (0.025 g, catalyst) were added and stirred at 700 rpm at the temperature reported in the table. After 6 h, the catalyst was separated by centrifugation and the reaction solution was analyzed by ^{1}H-NMR, using DMSO as deuterated solvent. *2,2-(dimethyl-[1,3]dioxan-4-yl)-methanol (solketal)*: ^{1}H-NMR (400 MHz, DMSO-d_6): δ = 4.78 (1H, t, -O*H*), 4.03 (1H, m, -C*H*-), 3.94 (1H, dd, -CH_2-CH-), 3.63 (1H, -CH_2-CH-), 3.42 (1H, m, -CH_2-OH), 3.35 (1H, m, -CH_2-OH), 1.30 (3H, s, -CH_3), 1.25 (3H, s, -CH_3).

Leaching tests: In a round-bottom flask, glycerol (921 mg, $1{\cdot}10^{-2}$ mol), absolute EtOH (0.70 mL) acetone (2.32 g, 4 equiv.) and Sn-NTs-B (0.025 g, catalyst) were added and heated at 50 °C under 700 rpm stirring. After 1 h, the catalyst was separated from the reaction mixture by hot filtration (~ 50 °C) and then centrifuged (4500 rpm, 5 min). A sample of the filtrate (0.4 mL) was dried under reduce pressure and analyzed by ^{1}H-NMR, using DMSO as solvent. The filtrate was kept at 50 °C for another 5 h. A second NMR analysis of the reaction mixture was then performed.

Recycling tests at 50 °C: In a round-bottom flask, glycerol (1.84 g, $2{\cdot}10^{-2}$ mol), acetone (4 equiv.), Sn-NTs-B catalyst (60 mg), were added and stirred at 50 °C for 4 h. After this, EtOH was added to the reaction mixture and the catalyst was separated from the mixture by centrifugation (4500 rpm, 5 min). A sample of the supernatant was taken out, dried under reduce pressure and analyzed by ^{1}H-NMR. Then, the supernatant was carefully removed from the centrifuge tube and the catalyst was rinsed with EtOH and centrifuged (twice). After this, the catalyst was calcined in air at 550 °C for 2 h (heating rate: 2 °C min^{-1}). The subsequent catalytic tests were carried out by repeating this procedure from the beginning (the quantities were adapted in function of the mass of recovered catalyst).

Recycling tests at room temperature: In a round-bottom flask, glycerol (1.874 g, $2{\cdot}10^{-2}$ mol), acetone (4.646 g, 4 equiv.), Sn-NTs-B catalyst (120 mg), were added and stirred at room temperature (25 °C) for 6 h. After this, the catalyst was separated from the reaction mixture by centrifugation (4500 rpm, 5 min). A sample of the supernatant was taken out, dried under reduce pressure and analyzed by ^{1}H-NMR. Then, the supernatant was carefully removed from the centrifuge tube and the catalyst was rinsed with EtOH and centrifuged (twice). After this, the catalyst was calcined in air at 550 °C for 2 h (heating rate: 2 °C min^{-1}). The subsequent catalytic tests were carried out by repeating this procedure from the beginning (the quantities were adapted in function of the mass of recovered catalyst).

3. Results and discussion

Sn-silicates with 1D tubular structure (**Sn-NTs**) were synthesized adapting a procedure previously reported for the preparation of silica nanotubes [27]. In order to achieve a successful incorporation of tin as single sites in the silica architecture and avoid the formation of separated SnO_2 domains, the two inorganic precursors were simultaneously added dropwise to an aqueous solution of Pluronic F127 (see experimental section for more details). After reaction, the mixture was subjected to hydrothermal treatment (HT) under static condition for 24 h (**Sn-NTs-A**). However, it was previously reported [4] that in some cases the HT could be avoided without detrimental effects on the morphological and textural properties of the solids. In order to investigate the possibility to reduce both reaction time and energy consumption, an analogous sample was synthetized eliminating the additional HT step at 100 °C for 24 h (**Sn-NTs-B**). Both solids were characterized employing several techniques including transmission electron microscopy, N_2 physisorption, FT-IR spectroscopy and solid state nuclear magnetic resonance among others.

Transmission electron microscopy (TEM) study, performed on **Sn-NTs-A** and **-B** solids, revealed mainly the presence of nanotubes and a minor amount of nanospheres (Fig. 1a and c). The nanostructures exhibit an average diameter of about 20 nm with an inner porosity of c.a. 15 nm. A careful TEM investigation, performed on different regions of the samples, allows evidencing a homogeneous pore size distribution. After calcination, the appearance of nanostructures of reduced length was observed indicating that the thermal treatment resulted in a partial cleavage of some tubes into smaller fragments (Fig. 1b and d). It is important to underline that, in view of the future catalytic applications, the presence of short tubes may represent an advantage, since an even increased accessibility of reactant and products to/from the active sites could be achieved in presence of nanotubes with decreased length.

The textural properties of both solids after calcination were characterized through N_2 physisorption measurements (Fig. 2 and Table 1). Both materials exhibited high surface area (Table 1). The hysteresis loop observed can be considered as a combination of two different contributions due to presence of tubular structures as well to disordered cavities generates by the entangled nanotubes. This behavior is particularly evident in the case of **Sn-NTs-B** which displays a step-wise desorption branch at intermediate relative pressure typical of tubular structures open at both ends together with a sloping adsorption branch characteristic of heterogeneously distributed pores. The steep capillary condensation followed by a broad adsorption-desorption hysteresis loop may suggest that the cylindrical nanotubes interiors are also accessible via small gaps in the walls [27]. Due to the entangled nature of nanotubes the pore size distributions was estimated via the Barrett-Joyner-Halenda (BJH) using the Kruk-Jaroniec-Sayari (KJS) correction [28,29] (Fig. 2). Two distinct porosities can be clearly distinguished, the first and more defined contribution centered at around 14 nm could be attributed to the internal void of the 1D structure in agreement with the TEM observations, while the second broader band was ascribed to the irregular inter-tubular spaces.

Solid state ^{29}Si MAS-NMR analysis revealed the presence of a broad asymmetrical band centered at -105 ppm, which can be considered as an overlapping of three different contributions centered at -90, -100 and -110 ppm and corresponding respectively to $Si(OSi)_2OH_2$ (Q^2) $Si(OSi)_3OH$ (Q^3) and $Si(OSi)_4$ (Q^4) species. As expected, the degree of condensation, defined as $Q^4/\Sigma Q^n$, was lower than standard silica based particle with spherical structure [4] (Figure S1). This result may be considered as a consequence of the 1D morphology of the nanotubes which display a surface decorated with hydroxyl groups. The tin loading was quantified via inductively coupled plasma optical emission spectroscopy (ICP-OES), the Si/Sn ratios are reported in Table 1. For comparison all-silica nanotubes (Si-NTs) were synthesized as well and fully characterized (Table 1 and Figure S2).

It is known that the isomorphic substitution of silicon with a metal

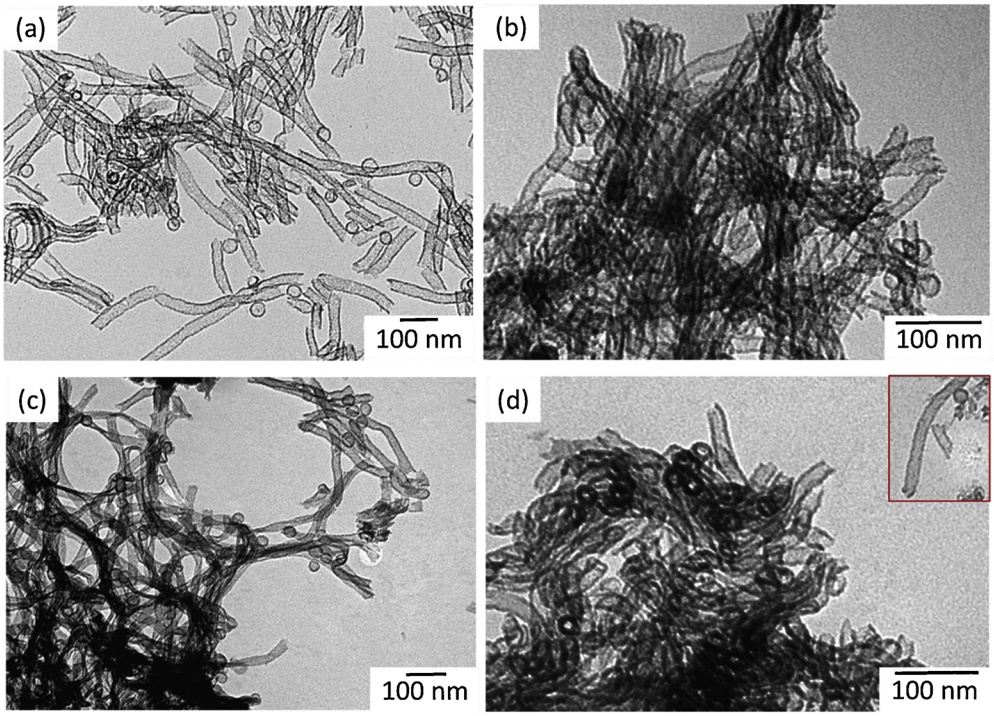

Fig. 1. TEM micrographs of: **Sn-NTs-A** before (a) and after calcination at 550 °C (b) and **Sn-NTs-B** before (c) and after calcination at 550 °C (d).

center in tetrahedral coordination within the SiO_2 network does not represent an easy achievement. Various parameters may influence the metal insertion including temperature, pH, nature and modality of addition of the inorganic precursors among others. The lower amount of tin in the silica nanotubes compared to other porous silica structures previously reported in the literature could be ascribed to the high acidity of the synthesis medium [30]. Shah et al. observed a similar behavior for the synthesis of Sn-SBA-15 solids [31]. Increasing amount of Sn in the synthesis mixture did not allow higher insertion of metal in the tubular structure. However, for the selected application, the amount of Sn determined experimentally is more than enough to ensure a good catalytic activity.

More importantly, the insertion of Sn in tetrahedral coordination should be carefully addressed. In order to deal with this objective solid state ^{119}Sn NMR experiments were performed as well (Fig. 3).

It is known [32,33] that the isomorphic substitution of Si with Sn in a silica framework is characterized by the appearance in ^{119}Sn NMR spectra of a band centered at around −700 ppm which can be attributed to tetrahedral coordinated tin atoms connected to four silicon through oxygen bridges or to partially hydrated intra-framework Sn species. Whereas, extra-framework SnO_2 nanoparticles would give a signal presenting a maximum at around −600 ppm. In the case of **Sn-NTs-A** a broad band shifted at higher frequencies is observed indicating

Table 1
Properties of **Si-NTs**, **Sn-NTs-A** and **Sn-NTs-B** materials.

Entry	Material	Time and Temperature of the synthesis	Surface area ($m^2\ g^{-1}$)[a]	PD (nm)[b]	Si/Sn[c]
1	Si-NTs	24 h 11 °C + 24 h 100 °C	656	13	_
2	Sn-NTs-A	24 h 11 °C + 24 h 100 °C	763	15	133
3	Sn-NTs-B	24 h 11 °C	754	13	135

[a] S_{BET} - specific surface area calculated from adsorption data in relative pressure range of 0.05-0.20 p/p_0 for all materials.
[b] BJH-KJS pore diameter.
[c] Determined by number of moles of Sn calculated from ICP-OES analysis for the calcined materials. Theoretical Si/Sn ratio of 37.

the presence of a combination of intra- and extra-framework tin species (Fig. 3a). On the other hand, **Sn-NTs-B** mainly displays tin inserted as single site (Fig. 3b) even if, due to the broad linewidth, the presence of a minor contribution of extra-framework SnO_2 cannot be completely excluded. This result suggests that the additional hydrothermal treatment leads to the formation of tin oxides domains with a detrimental effect on the insertion of tin as single site. This behavior could be ascribed to the strong acid conditions of the synthesis solution which, in combination with the relatively high temperature (100 °C) of the

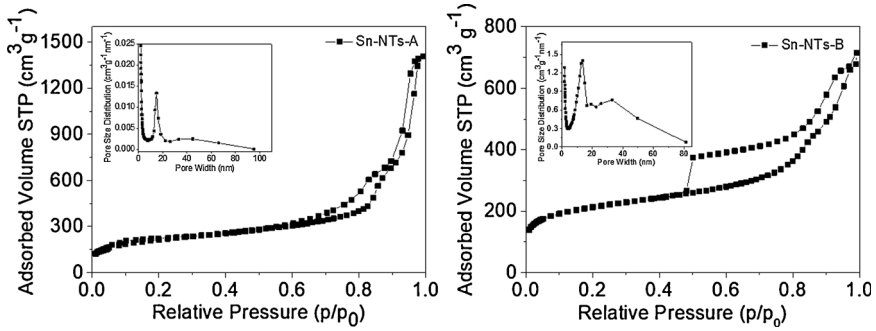

Fig. 2. Nitrogen adsorption-desorption isotherms of materials **Sn-NTs-A** and **Sn-NTs-B**.

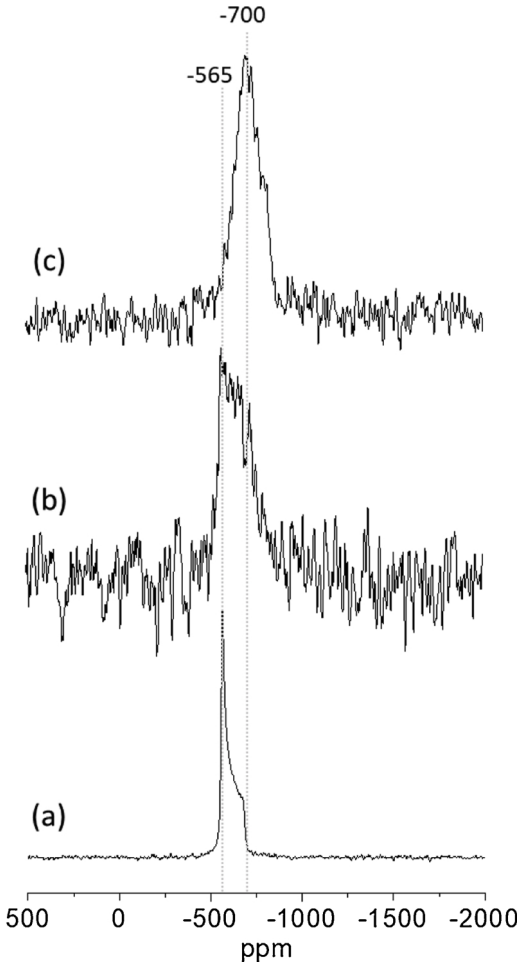

Fig. 3. Solid state ^{119}Sn NMR spectra recorded in static conditions of SnO_2 (a), materials **Sn-NTs-A** (b) and **Sn-NTs-B** (c).

hydrothermal treatment, could cause a migration of the intra-framework tin species to external surface through a process similar to the extensively described dealumination [34]. It is known [35] that zeolites can be dealuminated using high temperature steam or at more moderated temperatures (30 to 100 °C) in presence of elevated concentrations of mineral acids. On the other side, the insertion of Sn in SBA-15 matrix was successfully achieved using milder reaction conditions in terms of acidity (e.g. the HCl auto-generated from the hydrolysis of the $SnCl_4$ precursor) [36]. However, similar conditions cannot be applied in the present synthesis since the formation of tubular structure requires very low pH. Hence, Sn-nanotubes obtained without the additional hydrothermal treatment (sample B) constitute the best compromise between the acid conditions needed to obtain the 1D structures and the insertion of Sn as single site.

Moreover, this procedure allows obtaining a potentially better solid in a shorter synthesis time. The main reason behind the isomorphic substitution of silicon with tin is the generation of the appropriate balance of Lewis/ Brønsted acidity to promote both above mentioned reactions (see introduction). From the analysis of ^{119}Sn NMR data, it would be reasonable to suppose that **Sn-NTs-B** should display a higher amount of acid sites, hence better catalytic performances, compared to **Sn-NTs-A**.

In order to investigate the acidic properties, in term of acid site nature and concentration, the samples were studied via FT-IR of adsorbed ammonia (basic molecular probe), which can interact both with Brønsted (surface hydroxyls) and Lewis (surface Sn(IV)) sites.

FT-IR difference spectra (1700-1300 cm^{-1} range) of ammonia adsorption on both **Sn-NTs-A** and **Sn-NTs–B** are shown in Fig. 4 (a and b). The absorption band at 1635 cm^{-1} corresponds to the bending mode of NH_3 molecules H-bonded to hydroxyl groups, whereas the broad signal at around 1460 cm^{-1} is due to the bending mode of NH_4^+ ions resulting from proton-transfer reaction from Brønsted acidic groups. This suggests that the incorporation of Sn within the nanotube framework is able to provide Brønsted sites acid enough to protonate NH_3. On the contrary, the surface hydroxyls of pure silica materials interact with NH_3 via hydrogen-bonding without proton transfer. The intensity of the band ascribed to ammonium ion is significantly higher and broader for **Sn-NTs-B** compared to **Sn-NTs-A**, suggesting that the surface of the sample prepared without hydrothermal treatment is characterized by a larger population of hydroxyl groups. The larger broadness and the blue-shift of the ammonium band for **Sn-NTs-B** is attributed to the multiple lateral interactions of ammonium species with neighboring OH groups, which are more abundant for this system. Moreover, the spectra related to **Sn-NTs-B** reveal an additional component at around 1550 cm^{-1} which, based on the literature, [37] can be assigned to N—H bending vibration of Si-NH_2 species formed through reaction of strained siloxane bridges with ammonia. This reactivity is usually observed on amorphous silica-based materials upon treatment at high outgassing temperatures (700–800 °C). Here, although the lower outgassing temperature (400 °C) a similar assignment for the band is proposed. The peculiar nanotubular morphology of the investigated samples could cause the presence of strained reactive siloxane bridged as a consequence of the curvature of the surface.

For both samples, a shoulder at around 1610 cm^{-1} ascribed to ammonia molecule adsorbed on surface unsaturated cations acting as Lewis sites was observed.

Fig. 4c reports a comparison between the difference spectra of **Sn-NTs-A** and **Sn-NTs-B** after a prolonged outgassing at room temperature. For both samples the characteristic signal of NH_4^+ ions became less intense upon outgassing (reversible proton transfer), the absorption band attributed to NH_3 physisorbed on silanols (1635 cm^{-1}) decreased in intensity and was red-shifted up to 1606 cm^{-1} for **Sn-NTs-A** and 1610

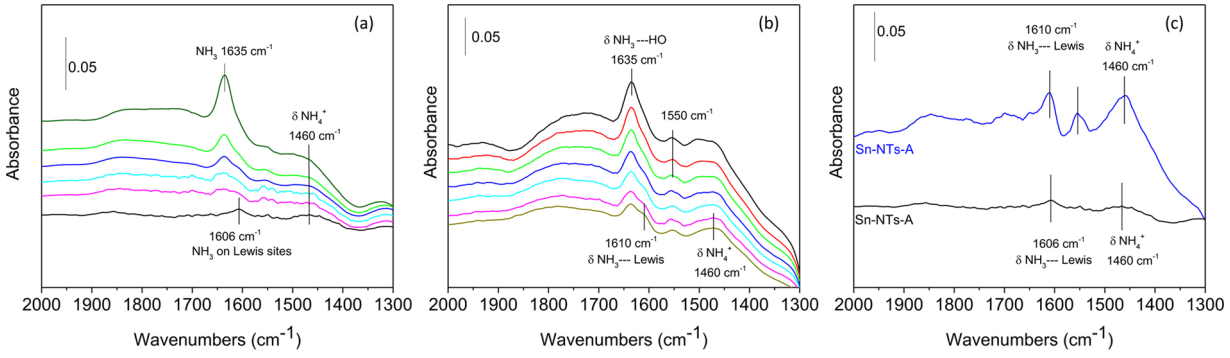

Fig. 4. Difference FT-IR spectra of NH_3 dosages on **Sn-NTs-A** (section a) and **Sn-NTs-B** (section b) and after prolonged outgassing (section c).

cm^{-1} for **Sn-NTs-B** for the fully outgassed samples (residual pressure $< 1{\cdot}10^{-3}$).

The band at 1550 cm^{-1} ascribed to Si-NH_2 is still clearly discernible in the spectrum of **Sn-NTs-B**, in agreement with the proposed assignation. It is evident that upon the same outgassing time the residual bands for **Sn-NTs-B** are significantly more intense than those of **Sn-NTs-A**, evidencing the larger population of Brønsted and Lewis acidic sites for the sample that did not undergo hydrothermal treatment. Furthermore, the residual bands assigned to ammonia on Lewis sites is at higher frequency for sample **Sn-NTs-B** (blue curve) compared to that recorded on **Sn-NTs-A** (black curve), which indicates for the former the presence of Lewis sites with average higher acidic strength compared to the latter [38].

On the basis of the characterizations results discussed above, it can be evidenced that tin-silica nanotubes present favorable features in the perspective of catalytic applications. The combination of acid sites, high surface area and the accessible pores are expected to have a positive impact on the performances of the materials. The catalytic activity of the **Sn-NTs** were initially investigated selecting the conversion of dihydroxyacetone (DHA) into ethyl lactate (EL) as target reaction. To allow a meaningful comparison between the two solids, as well as with reference catalysts reported in the literature, the activity was compared in term of turnover frequency (TOF, defined as moles of DHA converted/ moles of Sn x time(h)). The reaction time was selected in order to be far enough from the full DHA conversion. Two blank tests were initially carried out (Table 2) evidencing that in absence of catalyst no conversion is achieved (Table 2, entry 1) and, more importantly, that silica tubes are not acid enough to promote the conversion of DHA into EL (Table 2, entry 2). The catalytic tests performed with Sn-silica nanotubes evidenced that these materials are active catalysts for the selected reaction (Table 2, entries 3–4). As expected, **Sn-NTs-B** displayed enhanced catalytic performances than the analogous **Sn-NTs-A**. Since both morphology and textural properties of the materials are similar, these results could be ascribed to the better insertion of tin within silica framework in the case of **Sn-NTs-B** and to the consequent higher acidity of this material. It is important to underline that the best solid displays excellent TOF, higher than other Sn-based silica materials previously reported in literature (compare entries 3,4 with 5–7). Moreover, **Sn-NTS-B** presents outstanding performances compared to other catalysts bearing Ga and Zr inserted as single site (compare entries 3,4 with 8,9). A preparative test with **Sn-NTs-B** material was performed as well. Under optimized reaction conditions, (see experimental part) a high conversion (c.a. 90%) and a total selectivity (> 99%) were successfully achieved. The absence of leaching of catalytic active species was proved through a hot filtration experiment (Fig. 5). After 1 h reaction the catalyst was removed via hot filtration and the filtrate was left to react under the same conditions for additional 5 h. As can be seen from the figure the EL yield remains constant over time, proving that the reaction was performed in the presence of a true heterogeneous catalyst.

The second target reaction is represented by the acetalization of glycerol with acetone to produce solketal. Only the most active **Sn-NTs-B** was tested as catalyst for this reaction. In principle, the acetalization reaction can yield both five and six-membered ring compounds: (2,2-dimethyl-1,3-dioxolan-4-yl) methanol simply called solketal and (2,2-dimethyl-1,3-dioxan-5-ol) called acetal. Recently, one of the best solketal yield reported in the literature was achieved employing an acetone to glycerol ratio equal to 4:1 [41]. Hence, this ratio was selected to screen the catalytic performance of **Sn-NTs-B**. The tests were carried out under solvent free conditions varying the temperature, reaction time and amount of catalyst. Blank experiments performed at 80 °C for 6 h in the absence of catalyst (Table 3, entry 1) or with silica nanotubes (Table 3, entry 2), resulted in both cases in a very low glycerol conversion (c.a. 7%). Under the same reactions conditions, **Sn-NTs-B** catalyst displayed excellent catalytic performance, demonstrated not only by the high conversion and selectivity toward solketal, but also by the very high turnover frequency, equal to 378 (Table 3, entry 3).

The high TOF represents a clear indication of the high activity of the tubular structures, however the absolute values of turnover frequency are meaningless without comparison with literature data. Since several articles report the use of solvents, in order to allow a meaningful comparison with reference solids an additional catalytic test employing t-butanol as solvent was performed. The results resumed in Table 3 evidence the higher catalytic performance of **Sn-NTs-B** respect to Sn-based solids (entries 5,6) and other metal-containing silicates reported in literature (entries 7–9) [22,40]. This result further evidences the excellent performances of the nanotubes solids.

In view of sustainable processes, the decrease of the reaction temperature represents a key aspect. To this purpose, two additional tests at 50 and 25 °C (Fig. 6) were implemented. It is important to underline

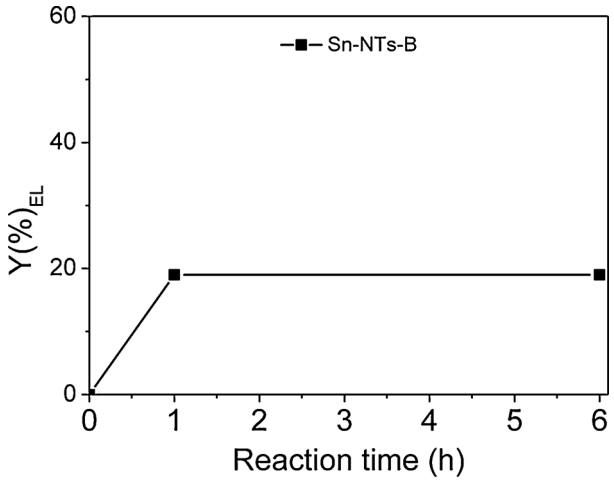

Fig. 5. Leaching tests for material **Sn-NTs-B**: yield of EL after 1 h and 6 h (catalyst removed). Reaction conditions: 2.5 mL 0.4 M DHA in EtOH, 50 mg of catalyst, 6 h at 90 °C.

Table 2
Conversion of DHA to ethyl lactate catalyzed by **Sn-NTs** materials.

Entry	Catalyst	Si/M	$Yield_{EL}$ (%)	$Conv._{DHA}$ (%)	$Sel._{EL}$ (%)	TOF	Reference
1	Si-NTs	-	-	-	-	-	This work
2	No catalyst	-	-	-	-	-	This work
3	Sn-NTs-A[a]	133	13	34	38	17	This work
4	Sn-NTs-B[a]	135	34	56	63	30	This work
5	Sn-MCM-41	49	30	32	94	7	Li et al. [39]
6	XS-Sn-MCM-41	63	44	64	69	17	Li et al. [14]
7	Sn-TUD-1	51	27	30	90	6	Li et al. [40]
8	XS-Ga-MCM-41-H	15	12	20	60	2	Collard et al. [13]
9	Zr-TUD-1	51	28	31	91	7	Li et al. [40]

Reaction conditions: 50 mg of catalyst, 5 mL of 0.4 M DHA solution in absolute EtOH, 6 h at 90 °C.
[a] TOF values calculated from moles of Sn obtained by ICP-OES analysis of the calcined materials.

Table 3
Condensation of glycerol with acetone yielding solketal by **Sn-NTs** materials.

Entry	Catalyst	Solvent	$Yield_{SK}$ (%)	$Sel._{SK}$ (%)	TOF	Reference
1	No catalyst	_	7	99	_	This work
2	Si-NTs	_	8	99	_	This work
3	Sn-NTs-B[a]	_	58	97	378	This work
4	Sn-NTs-B[a]	t-butanol	26	96	185	This work
5	Sn-MCM-41	t-butanol	42	99	102	Li et al. [22]
6	Sn-TUD-1	t-butanol	44	99	94	Li et al. [40]
7	XS-Ga-MCM-41-L	t-butanol	25	99	60	Collard et al. [13]
8	Zr-TUD-1	t-butanol	46	99	127	Li et al. [22]
9	Al-TUD-1	t-butanol	28	99	61	Li et al. [22]

Reaction conditions: 0.920 g of glycerol (0.01 mol), 4 eq. of acetone, catalyst at 6 h.

[a] TOF values calculated from moles of Sn obtained by ICP-OES analysis of the calcined materials.

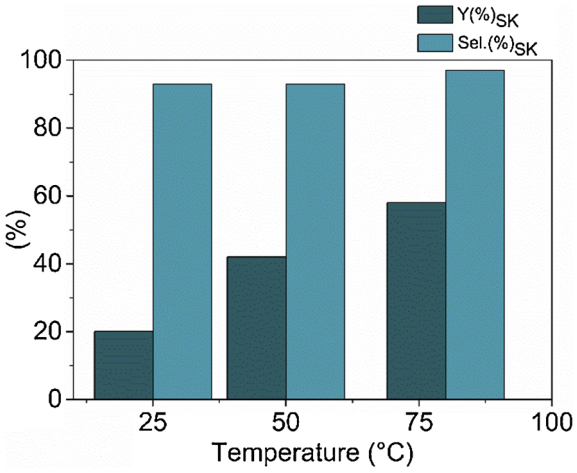

Fig. 6. Reaction conditions: 0.920 g of glycerol (0.01 mol), 4 eq. of acetone, 25 mg of **Sn-NTs-B** for 6 h.

that the overall catalytic performances (conversion and selectivity) did not suffer of a relevant decrease when the test was performed at 50 °C. Surprisingly, when glycerol acetalization was performed at 25 °C, a moderate solketal yield (20%) was still observed despite the challenging conditions. The decrease of activity may be also ascribed to the intrinsic difficulties of the selected reaction conditions due to the high viscosity of glycerol which (at 25 °C) can be also responsible for diffusion limitations.

The effect of the amount of catalyst was investigated as well and the most representative tests are reported in Table 4. At 80 °C a surprisingly high turnover number (TON, defined as moles of glycerol converted/

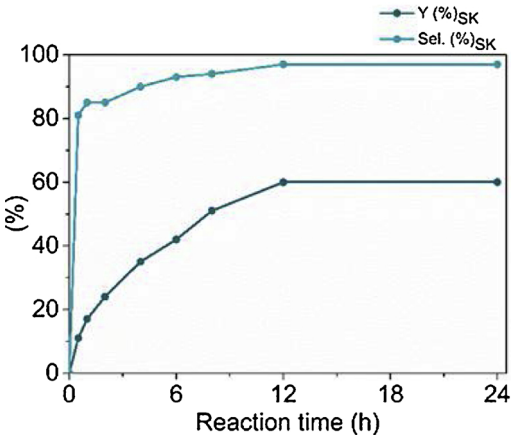

Fig. 7. Kinetic study with **Sn-NTs-B**. Reaction conditions: glycerol (0.01 mol), 4 eq. of acetone at 50 °C.

moles of Sn) equal to 3892 (entry 1) was obtained lowering the amount of catalyst to only 10 mg. However, raising the catalyst mass loading at 25 did not result in a proportional improvement in the conversion. A similar behavior was observed when performing the reaction at 50 °C (entries 3–6). A plateau is reached around 60% yield of solketal. Comparable results were observed by Nanda et al. [16,42]. In this context, the authors reported a study based on the influence of the catalyst amount (Amberlyst-35) on glycerol ketalization reaction. To support this analysis a kinetic investigation was also performed by monitoring the formation of the solketal over time in the range of 30 min to 24 h (Fig. 7). All tests were carried out at 50 °C, using 25 mg of **Sn-NTs-B** as catalyst (Fig. 7).

The analysis of these data allows evidencing that at about 60% solketal yield an equilibrium is reached and further improvements of the catalysts performances are not possible in absence of modifications of some parameter (e.g. reactants addition or product removal) which can alter the equilibrium itself.

In line with these considerations, not all the TOF reported in Table 4 are truly representative of the catalyst performances and most of them (e.g. entries 2, 5 and 6) underestimate its activity. Hence, a more representative TOF value was recalculated at the very early stage of the reaction (Table 4, entries 7–9).

All the previously reported results suggest that a reaction temperature of 50 °C can be selected as best compromise between catalytic activity and sustainability (reduced energy consumption). Hence, the last screenings were performed at this temperature. The heterogeneous nature of catalyst **Sn-NTs-B** was proved by hot filtration experiment (Fig. 8a). As can be clearly observed in the figure, the yield of solketal did not increase after removal of the catalyst from the reaction mixture, indicating the absence of leaching of active sites.

Table 4
Condensation of glycerol with acetone yielding solketal by **Sn-NTs-B** material.

Entry	Amount (mg)	Temperature (°C)	Time (h)	$Yield_{SK}$ (%)	$Sel._{SK}$ (%)	Productivity	TON	TOF
1	10	80	6	42	95	39	3892	649
2	25	80	6	58	97	21	2267	378
3	10	50	6	20	84	18	1565	261
4	25	50	6	42	93	15	1377	230
5	50	50	6	61	98	11	1000	167
6	100	50	6	63	99	6	516	86
7	25	50	0.5	11	81	4	344	688
8	25	50	1	17	85	6	532	532
9	25	50	2	24	85	9	751	376

Reaction conditions: 0.920 g of glycerol (0.01 mol), 4 eq. of acetone, catalyst. TON and TOF values calculated from moles of Sn obtained by ICP-OES analysis of the calcined material.

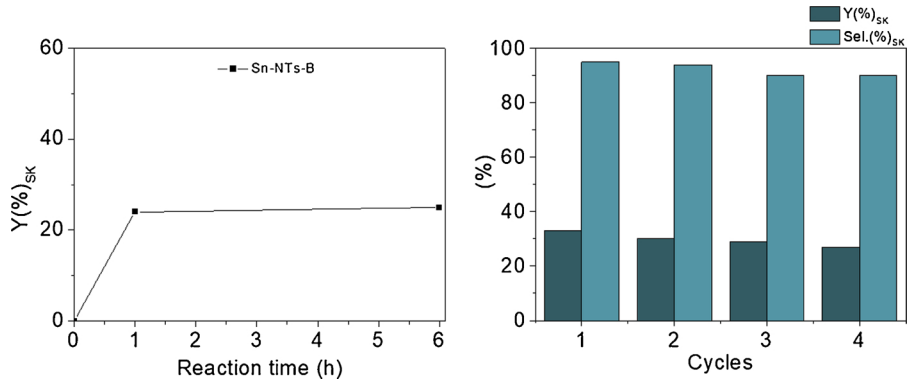

Fig. 8. Hot filtration experiment (a) and recycling tests (b) with **Sn-NTs-B** material. Reaction conditions: 0.920 g of glycerol (0.01 mol), 25 mg of catalyst, 4 eq. of acetone (a); 1.840 g of glycerol (0.02 mol), 60 mg of catalyst, 4 eq. of acetone, 50 °C for 4 h (b).

The reusability of **Sn-NTs-B** was investigated at intermediate solketal yield far enough from glycerol equilibrium conversion (Fig. 8b). After each run, the catalyst was reactivated by a short calcination treatment before the following catalytic cycle (see experimental part). Only a minor decrease in term of yield and selectivity was observed upon successive reuses, suggesting that tin-silica tubes were stable in the reaction conditions. As reported previously [13], the calcination treatment is of fundamental importance to restore the activity of the catalysts employed in the conversion of glycerol. This behavior was ascribed to the adsorption of organic species on the surface of the catalyst, which cannot be efficiently removed by washing procedures. The absence of tin leaching was again supported by ICP-OES analysis on the regenerated catalyst. After the fourth cycle, no difference was observed in term of Si/Sn ratio between the fresh and reused catalyst (Table S1). Moreover, the full characterization of the catalyst after recycle via TEM, N_2 physisorption and ^{119}Sn NMR (Figures S3 and S4) did not display substantial differences with the fresh solid hence supporting further the stability of the **Sn-NTs-B** material under the selected reactions conditions.

4. Conclusions

A novel silica based solid displaying a 1D tubular structure and bearing Sn inserted as single site in the framework was successfully prepared for the first time. The synthesis procedure was optimized in order to achieve the isomorphic substitution of silicon through a relatively short protocol.

The solid was fully characterized via transmission electron microscopy, ICP-OES analysis, ^{29}Si and ^{119}Sn solid state NMR spectroscopy. Specific surface area and the pore dimensions were determined through N_2 physisorption measurements. Due to the entangled organization of the Sn-nanotubes the standard Barrett-Joyner-Halenda (BJH) pore size distributions was implemented using the Kruk-Jaroniec-Sayari (KJS) correction. The optimized material exhibited outstanding catalytic activity in particular in the direct conversion of glycerol to solketal. This behavior was ascribed to the good insertion of tin within silica framework as well as to the high acidity of the **Sn-NTs** as proved by FT-IR measurements of ammonia adsorption. The exceptional catalytic performance of the solid allows decreasing the reaction temperature with good results in terms of solketal yield. Moreover, the catalyst proved to be stable under the selected conditions and reusable in multiple runs. The robustness of the Sn-silica nanotubes was also supported via full characterization of the solid after the 4th cycle.

Acknowledgements

Authors acknowledge the 'Communauté française de Belgique' for the financial support – including the Postdoctoral fellowships of L.A. Bivona and the PhD fellowship of A. Vivian – through the ARC programme (15/20-069). This research used resources of the Plateforme Technologique "Physico-Chemical Characterization" – PC^2 and "Morphology and Imaging"- MORPH-IM located at the University of Namur.

Appendix A. Supplementary data

Supplementary material related to this article can be found, in the online version, at doi:https://doi.org/10.1016/j.apcatb.2019.01.085.

References

[1] P.T. Anastas, J.C. Warner, 12 Principles of Green Chemistry. Green Chemistry: Theory and Practice, Oxford Univ. Press, New York, 1998 By Permis. Oxford Univ. Press.
[2] N.R. Shiju, V.V. Guliants, Recent developments in catalysis using nanostructured materials, Appl. Catal. A Gen. 356 (2009) 1–17, https://doi.org/10.1016/j.apcata.2008.11.034.
[3] X. Sheng, B. Wouters, T. Breugelmans, A. Hubin, I.F.J. Vankelecom, P.P. Pescarmona, Cu/Cu$_x$O and Pt nanoparticles supported on multi-walled carbon nanotubes as electrocatalysts for the reduction of nitrobenzene, Appl. Catal. B Environ. 147 (2014) 330–339, https://doi.org/10.1016/j.apcatb.2013.09.006.
[4] N. Godard, X. Collard, A. Vivian, L.A. Bivona, S. Fiorilli, L. Fusaro, C. Aprile, Rapid room temperature synthesis of tin-based mesoporous solids: influence of the particle size on the production of ethyl lactate, Appl. Catal. A Gen. 556 (2018) 73–80, https://doi.org/10.1016/j.apcata.2018.02.014.
[5] E. Czárán, Introduction to zeolite science and practice, React. Kinet. Catal. Lett. 45 (1991) 161–163, https://doi.org/10.1007/BF02078624.
[6] A. Corma, From microporous to mesoporous molecular sieve materials and their use in catalysis, Chem. Rev. 97 (1997) 2373–2420, https://doi.org/10.1021/cr960406n.
[7] A. Taguchi, F. Schüth, Ordered mesoporous materials in catalysis, Microporous Mesoporous Mater. 77 (2005) 1–45, https://doi.org/10.1016/j.micromeso.2004.06.030.
[8] S. Telalović, A. Ramanathan, G. Mul, U. Hanefeld, TUD-1: synthesis and application of a versatile catalyst, carrier, material…, J. Mater. Chem. 20 (2010) 642–658, https://doi.org/10.1039/b904193a.
[9] M. Adachi, T. Harada, M. Harada, Formation of huge length silica nanotubes by a templating mechanism in the laurylamine/tetraethoxysilane system, Langmuir 15 (1999) 7097–7100, https://doi.org/10.1021/la9904859.
[10] G. Farid, M. Kruk, Silica nanotubes with widely adjustable inner diameter and ordered silicas with ultralarge cylindrical mesopores templated by swollen micelles of mixed pluronic triblock copolymers, Chem. Mater. 29 (2017) 4675–4681, https://doi.org/10.1021/acs.chemmater.6b05504.
[11] M. Mandal, M. Kruk, Family of single-micelle-templated organosilica hollow nanospheres and nanotubes synthesized through adjustment of organosilica/surfactant ratio, Chem. Mater. 24 (2012) 123–132, https://doi.org/10.1021/cm202136r.
[12] S. Zhang, H. Wang, M. Li, J. Han, X. Liu, J. Gong, Molecular heterogeneous catalysts derived from bipyridine-based organosilica nanotubes for C–H bond activation, Chem. Sci. 8 (2017) 4489–4496, https://doi.org/10.1039/C7SC00713B.
[13] X. Collard, L. Li, W. Lueangchaichaweng, A. Bertrand, C. Aprile, P.P. Pescarmona, Ga-MCM-41 nanoparticles: synthesis and application of versatile heterogeneous catalysts, Catal. Today 235 (2014) 184–192, https://doi.org/10.1016/j.cattod.2014.02.055.
[14] L. Li, X. Collard, A. Bertrand, B.F. Sels, P.P. Pescarmona, C. Aprile, Extra-small porous Sn-silicate nanoparticles as catalysts for the synthesis of lactates, J. Catal. 314 (2014) 56–65, https://doi.org/10.1016/j.jcat.2014.03.012.
[15] N. Godard, A. Vivian, L. Fusaro, L. Cannavicci, C. Aprile, D.P. Debecker, High-yield

synthesis of ethyl lactate with mesoporous tin silicate catalysts prepared by an aerosol-assisted sol–gel process, ChemCatChem. 9 (2017) 2211–2218, https://doi.org/10.1002/cctc.201601637.
[16] M.R. Nanda, Y. Zhang, Z. Yuan, W. Qin, H.S. Ghaziaskar, C. Charles, Catalytic conversion of glycerol for sustainable production of solketal as a fuel additive: a review, Renew. Sustain. Energy Rev. 56 (2016) 1022–1031, https://doi.org/10.1016/j.rser.2015.12.008.
[17] C.J.A. Mota, C.X.A. Da Silva, N. Rosenbach, J. Costa, F. Da Silva, Glycerin derivatives as fuel additives: The addition of glycerol/acetone ketal (solketal) in gasolines, Energy Fuels 24 (2010) 2733–2736, https://doi.org/10.1021/ef9015735.
[18] M.J. Climent, A. Corma, A. Velty, Synthesis of hyacinth, vanilla, and blossom orange fragrances: the benefit of using zeolites and delaminated zeolites as catalysts, Appl. Catal. A Gen. 263 (2004) 155–161, https://doi.org/10.1016/j.apcata.2003.12.007.
[19] J. Deutsch, A. Martin, H. Lieske, Investigations on heterogeneously catalysed condensations of glycerol to cyclic acetals, J. Catal. 245 (2007) 428–435, https://doi.org/10.1016/j.jcat.2006.11.006.
[20] L. Roldán, R. Mallada, J.M. Fraile, J.A. Mayoral, M. Menéndez, Glycerol upgrading by ketalization in a zeolite membrane reactor, Asia-Pac. J. Chem. Eng. 4 (2009) 279–284, https://doi.org/10.1002/apj.243.
[21] G. Vicente, J.A. Melero, G. Morales, M. Paniagua, E. Martín, Acetalisation of bioglycerol with acetone to produce solketal over sulfonic mesostructured silicas, Green Chem. 12 (2010) 899–907, https://doi.org/10.1039/b923681c.
[22] L. Li, T.I. Korányi, B.F. Sels, P.P. Pescarmona, Highly-efficient conversion of glycerol to solketal over heterogeneous Lewis acid catalysts, Green Chem. 14 (2012) 1611–1619, https://doi.org/10.1039/c2gc16619d.
[23] A. Corma, S. Iborra, A. Velty, Chemical routes for the transformation of biomass into chemicals, Chem. Rev. 107 (2007) 2411–2502, https://doi.org/10.1021/cr050989d.
[24] R.E. Drumright, P.R. Gruber, D.E. Henton, Polylactic acid technology, Adv. Mater. 12 (2000) 1841–1846, https://doi.org/10.1002/1521-4095(200012)12:23<1841::AID-ADMA1841>3.0.CO;2-E.
[25] R.A. Sheldon, Green solvents for sustainable organic synthesis: state of the art, Green Chem. 7 (2005) 267, https://doi.org/10.1039/b418069k.
[26] P.P. Pescarmona, K.P.F. Janssen, C. Delaet, C. Stroobants, K. Houthoofd, A. Philippaerts, C. De Jonghe, J.S. Paul, Pa. Jacobs, B.F. Sels, Zeolite-catalysed conversion of C3 sugars to alkyl lactates, Green Chem. 12 (2010) 1083–1089, https://doi.org/10.1039/b921284a.
[27] L. Huang, M. Kruk, Versatile surfactant/swelling-agent template for synthesis of large-pore ordered mesoporous silicas and related hollow nanoparticles, Chem. Mater. 27 (2015) 679–689, https://doi.org/10.1021/cm5028749.
[28] M. Kruk, M. Jaroniec, A. Sayari, Adsorption study of surface and structural properties of MCM-41 materials of different pore sizes, J. Phys. Chem. B 101 (1997) 583–589, https://doi.org/10.1021/jp962000k.
[29] M. Jaroniec, L.A. Solovyov, Improvement of the Kruk-Jaroniec-Sayari method for pore size analysis of ordered silicas with cylindrical mesopores, Langmuir. 22 (2006) 6757–6760, https://doi.org/10.1021/la0609571.
[30] S. Wu, Y. Han, Y.C. Zou, J.W. Song, L. Zhao, Y. Di, S.Z. Liu, F.S. Xiao, Synthesis of heteroatom substituted SBA-15 by the “pH-adjusting” method, Chem. Mater. 16 (2004) 486–492, https://doi.org/10.1021/cm0343857.
[31] P. Shah, V. Ramaswamy, Thermal stability of mesoporous SBA-15 and Sn-SBA-15 molecular sieves: an in situ HTXRD study, Microporous Mesoporous Mater. 114 (2008) 270–280, https://doi.org/10.1016/j.micromeso.2008.01.013.
[32] K. Chaudhari, T.K. Das, P.R. Rajmohanan, K. Lazar, S. Sivasanker, A.J. Chandwadkar, Synthesis, characterization, and catalytic properties of mesoporous tin-containing analogs of MCM-41, J. Catal. 183 (1999) 281–291, https://doi.org/10.1006/jcat.1999.2394.
[33] M. Renz, T. Blasco, A. Corma, V. Fornés, R. Jensen, L. Nemeth, Selective and shape-selective Baeyer-Villiger oxidations of aromatic aldehydes and cyclic ketones with Sn-beta zeolites and H2O2, Chem. - A Eur. J. 8 (2002) 4708–4717, https://doi.org/10.1002/1521-3765(20021018)8:20<4708::AID-CHEM4708>3.0.CO;2-U.
[34] R. Xu, W. Pang, J. Yu, Q. Huo, J. Chen, Chemistry of Zeolites and Related Porous Materials: Synthesis and Structure, Wiley, 2010, https://doi.org/10.1002/9780470822371.
[35] Z. Yan, D. Ma, J. Zhuang, X. Liu, X. Liu, X. Han, X. Bao, F. Chang, L. Xu, Z. Liu, On the acid-dealumination of USY zeolite: A solid state NMR investigation, J. Mol. Catal. A Chem. 194 (2003) 153–167, https://doi.org/10.1016/S1381-1169(02)00531-9.
[36] P. Shah, A.V. Ramaswamy, K. Lazar, V. Ramaswamy, Direct hydrothermal synthesis of mesoporous Sn-SBA-15 materials under weak acidic conditions, Microporous Mesoporous Mater. 100 (2007) 210–226, https://doi.org/10.1016/j.micromeso.2006.10.042.
[37] M. Piumetti, M. Armandi, E. Garrone, B. Bonelli, An IR spectroscopy assessment of the surface acidity of mesoporous VO_x-SiO_2 catalysts, Microporous Mesoporous Mater. 164 (2012) 111–119, https://doi.org/10.1016/j.micromeso.2012.05.041.
[38] G. Busca, Heterogeneous catalytic materials, Heterog. Catal. Mater. (2014) 103–195, https://doi.org/10.1016/B978-0-444-59524-9.00006-7.
[39] L. Li, C. Stroobants, K. Lin, P.A. Jacobs, B.F. Sels, P.P. Pescarmona, Selective conversion of trioses to lactates over Lewis acid heterogeneous catalysts, Green Chem. 13 (2011) 1175, https://doi.org/10.1039/c0gc00923g.
[40] L. Li, D. Cani, P.P. Pescarmona, Metal-containing TUD-1 mesoporous silicates as versatile solid acid catalysts for the conversion of bio-based compounds into valuable chemicals, Inorg. Chim. Acta 431 (2015) 289–296, https://doi.org/10.1016/j.ica.2015.04.011.
[41] F.D.L. Menezes, M.D.O. Guimaraes, M.J. Da Silva, Highly selective $SnCl_2$-catalyzed solketal synthesis at room temperature, Ind. Eng. Chem. Res. 52 (2013) 16709–16713, https://doi.org/10.1021/ie402240j.
[42] M.R. Nanda, Z. Yuan, W. Qin, H.S. Ghaziaskar, M.A. Poirier, C.C. Xu, Thermodynamic and kinetic studies of a catalytic process to convert glycerol into solketal as an oxygenated fuel additive, Fuel 117 (2014) 470–477, https://doi.org/10.1016/j.fuel.2013.09.066.
[43] C. Cossement, J. Darville, J. Gilles, J.B. Nagy, Chemical shift anisotropy and indirect coupling in SnO_z and SnO, Magn. Reson. Chem. 30 (1992) 263–270, https://doi.org/10.1002/mrc.1260300313.